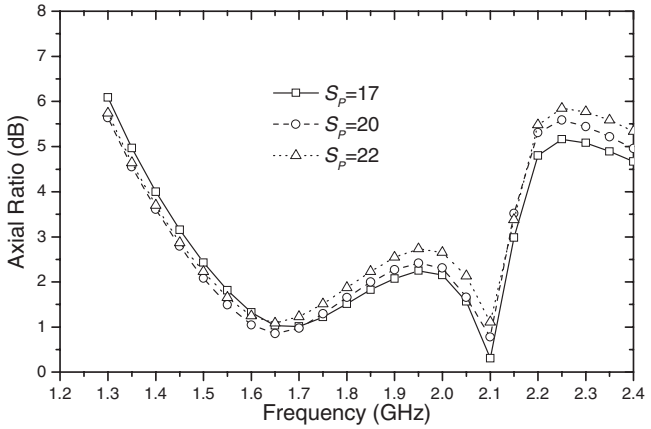

Figure 9 Effects of S_P on the AR of the proposed antenna versus frequency

ACKNOWLEDGMENTS

This work was supported by a grant from the Research Grants Council of the Hong Kong SAR, China [Project No. CityU122407], and strategic Research Grants of the City University of Hong Kong [Project No. 7002026].

REFERENCES

1. R.S. Elliott, Antenna theory and design, Prentice-Hall, Englewood, NJ, 1981.
2. I.-C. Deng, Q.-X. Ke, R.-J. Lin, and Y.-T. King, A circular CPW-fed slot antenna resonated by the circular loop for broadband circularly polarized radiation, Microwave Opt Technol Lett 50 (2008), 1423–1426.
3. Y. Murakami, A. Yoshida, K. Leda, and T. Nakamura, Rectangular loop antenna for circular polarization, Electron Commun Jpn 79 (1996), 42–51.
4. H. Scott and V.F. Fusco, Circular wire loop antenna with stepped wire diameter, Microwave Opt Technol Lett 34 (2002), 14–15.
5. M. Sumi, K. Hirasawa, and S. Song, Two rectangular loops fed in series for broadband circular polarization and impedance matching, IEEE Trans Antennas Propag 52 (2002), 551–554.
6. Y. Zhang and L. Zhu, CPS-fed printed dual spiral-loop strip antenna with circular polarization, Microwave Opt Technol Lett 46 (2005), 506–508.
7. Y. Zhang and L. Zhu, Printed dual spiral-loop wire antenna for broadband circular polarization, IEEE Trans Antennas Propag 54 (2006), 284–288.
8. R. Li, A. Traille, J. Laskar, and M.M. Tentzeris, Bandwidth and gain improvement of a circularly polarized dual-rhombic loop antenna, IEEE Antennas Wireless Propag Lett 5 (2006), 84–87.
9. R. Li, J. Laskar, and M.M. Tentzeris, Broadband circularly polarized rectangular loop antenna with impedance matching, IEEE Microwave Wireless Compon Lett 16 (2006), 52–54.
10. S.-G. Kim and K. Chang, Ultrawide-band transitions and new microwave components using double-sided parallel-strip lines, IEEE Trans Microwave Theory Tech 52 (2004), 2148–2152.
11. H.W. Ehrenspeck, A new class of medium-size high-efficiency reflector antennas, IEEE Trans Antennas Propag 22 (1974), 329–332.

GILBERT UPCONVERSION MIXERS USING SINGLE-BAND/DUAL-BAND LC CURRENT COMBINERS

Jin-Siang Syu,[1] Chinchun Meng,[1] Ying-Chieh Yen,[1] and Guo-Wei Huang[2]

[1] Department of Communication Engineering, National Chiao Tung University, Hsinchu, Taiwan, Republic of China

[2] National Nano Device Laboratories, Department of Electronics Engineering, National Chiao Tung University, Hsinchu 300, Taiwan, Republic of China; Corresponding author: gwhuang@mail.ndl.org.tw

Received 13 October 2008

ABSTRACT: *The 0.35-μm SiGe BiCMOS high linearity Gilbert upconverters are demonstrated in this article by utilizing NMOS and PMOS transconductance amplifiers (TCAs), respectively. To improve the linearity of a Gilbert upconverter, the IF input TCA is replaced by a bias-offset differential pair. A reactive LC current combiner is used as the load of the Gilbert mixer to double the output current. The upconverter with an NMOS TCA achieves the conversion gain of −4 dB, the OP_{1dB} of −11 dBm, and the OIP_3 of 5.5 dBm, whereas the other one with a PMOS TCA has the conversion gain, OP_{1dB}, and OIP_3 of −6 dB, −11 dBm, and 9.5 dBm, respectively. Furthermore, the LC current combiner can be extended to a dual-band version. The 2.4/5.7 GHz dual-band upconverter is also demonstrated in this work. The conversion gain at 2.4/5.7 GHz is −3/−3.5 dB with the OP_{1dB} of −15.5/−15 dBm and the OIP_3 of −2.5/−3 dBm, respectively.* © 2009 Wiley Periodicals, Inc.

Microwave Opt Technol Lett 51: 1718–1722, 2009; Published online in Wiley InterScience (www.interscience.wiley.com). DOI 10.1002/mop.24433

Key words: *SiGe BiCMOS; bias-offset; Gilbert mixer; transconductance amplifier (TCA); dual-band*

1. INTRODUCTION

Linearity requirement is an important issue in wireless transmitters. The passive mixers (including the resistive mixers [1] or the diode mixers [2]) are demonstrated with high linearity but severe loss. On the other hand, a Gilbert mixer topology is widely used in a wireless transceiver to avoid the severe loss at high frequencies. The current commutation mechanism of the Gilbert mixer core is highly linear and performs frequency translation. Moreover, the reactive load of a Gilbert mixer is used without any linearity degradation. Consequently, the linearity is restricted by the input and output stages.

A conventional Gilbert mixer has a poor linearity performance due to the use of a simple differential amplifier in the input stage. To improve the linearity of the input transconductance amplifier (TCA), the multi-tanh technique [3] is widely used for a bipolar-transistor-based TCA. There are also solutions for linearity improvement based on the square law I–V characteristics of the MOS transistors [4, 5]. However, the short channel effect degrades the linearity, especially when a large gate-to-source voltage is applied on the device with a shorter gate length in an advanced CMOS technology.

2. CIRCUIT DESIGN

The schematics of the Gilbert upconversion mixers with the NMOS-type and the folded PMOS-type input stages are shown in Figure 1. An upconverter consists of an input TCA, a current switching quad, and an output transimpedance amplifier (TIA).

2.1. Bias-Offset Transconductance Amplifier

The bias-offset differential pair [6] used in the input stage has the transconductance of $2kV_B$ if the MOS characteristic is still in the

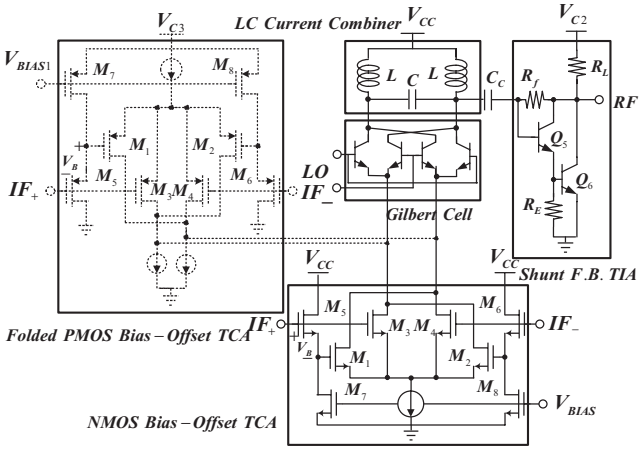

Figure 1 Schematic of the Gilbert upconverters with NMOS/PMOS-type bias-offset TCAs and a single-band LC current combiner

square-law regime with a long channel transfer function. The parameter k is the transconductance parameter of M_1–M_4 and V_B is the gate-to-source voltage drop of M_5–M_6 which provides a dc offset voltage for the two differential pairs of M_1–M_2 and M_3–M_4.

The drain saturation voltage is less than the gate-overdrive voltage if the short channel effect takes place. However, if the gate-overdrive voltage is still small, the MOS transistors are still in the long channel regime because the electric field is not large enough to saturate the drift velocity of the electrons. Because the PMOS transistor has a lower mobility than the NMOS transistor for the same size, the PMOS transistor is almost in the long channel regime even if the gate-overdrive voltage is large. The gate length of the NMOS transistors M_1–M_4 in the input stage of the first chip is 0.5 μm, whereas the gate length of the PMOS transistors M_1–M_4 of the other chip is 1 μm. For the lower mobility of the PMOS transistors, the widths of the PMOS transistors are designed much wider to achieve similar transconductance gain when compared with the NMOS upconverter. As a result, the IF bandwidth of the upconverter with a folded PMOS TCA is narrower than that with an NMOS TCA.

2.2. Gilbert Mixer Core with an LC Current Combiner

Instead of using the MOS transistors in the Gilbert switching quad with a large LO switching voltage requirement of $\sqrt{2V_{ov}}$ (gate-overdrive voltage), the bipolar transistors Q_1–Q_4 are utilized in this work with only about 0.1-V LO voltage swing requirement to make the current fully switch. The current commutation mechanism is highly linear and only performs the frequency translation. The differential output current of the Gilbert mixer is depicted as I_+ and I_- with the LC current combiner as shown in Figure 2. At the resonant frequency of $\omega_0 = 1/\sqrt{2LC}$, the input current I_+ reverses and thus the total output current doubles when compared to the single-ended output current of each path [7, 8].

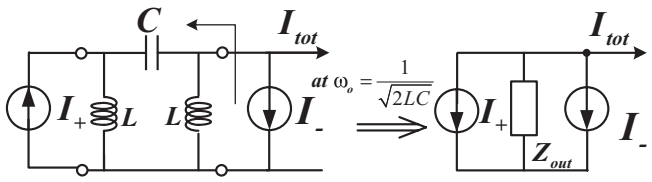

Figure 2 Block diagram of the LC current combiner and its equivalent circuit at the resonant frequency

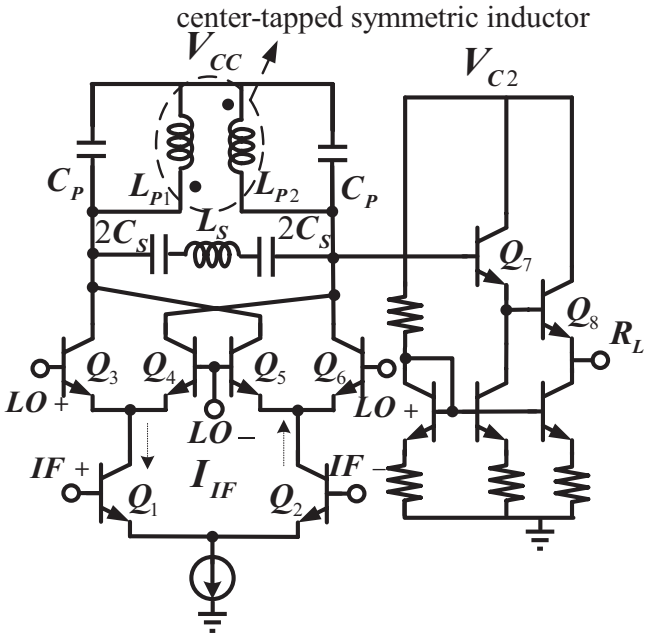

Figure 3 Schematic of the 2.4/5.7 GHz dual-band Gilbert upconverter with a dual-band LC current combiner

2.3. Shunt–Shunt Feedback Transimpedance Amplifier

The output shunt–shunt feedback TIA is used to translate the combined current output I_{tot} to the voltage signal. Moreover, the output impedance is reduced by the factor of $(1 + A\beta)$ for the shunt-type feedback and thus the output matching is easily

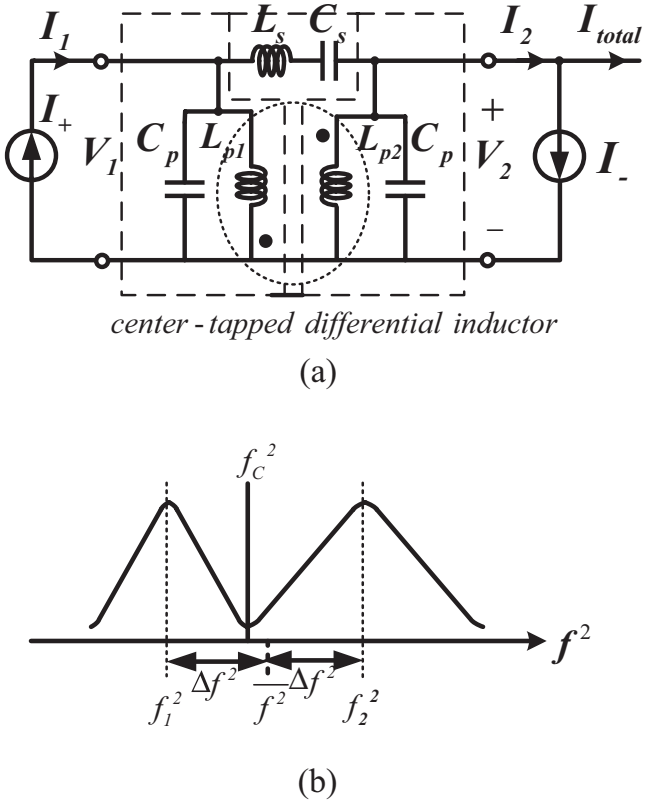

Figure 4 (a) dual-band prototype of the LC current combiner and (b) its current combining performance

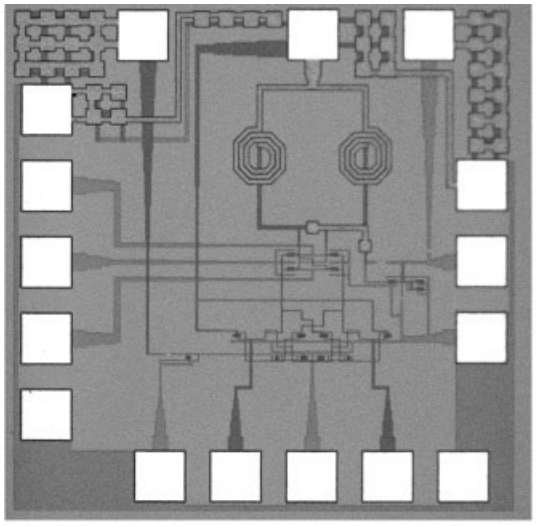

(a)

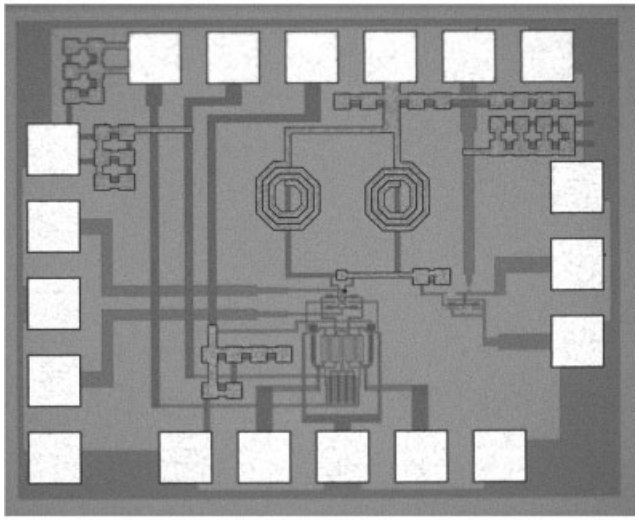

(b)

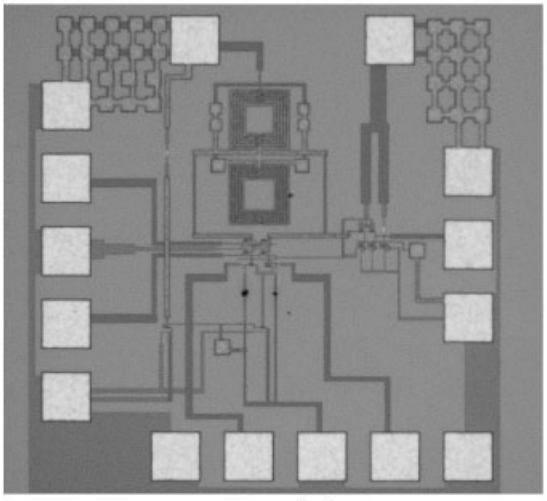

(c)

Figure 5 (a) Photograph of the SiGe BiCMOS high linearity Gilbert upconverter using an NMOS TCA and an LC current combiner (b) using a PMOS TCA and the same current combiner (c) dual-band Gilbert upconverter with dual-band LC current combiner

achieved. The 20-GHz bandwidth of the feedback TIA is designed with strong feedback to reduce the nonlinearity effect [9].

Moreover, the schematic of the 2.4/5.7 GHz dual-band upconverter using dual-band LC current combiner is shown in Figure 3. Figure 4 shows a dual-band resonator consisting of two parallel resonators [L_P ($= L_{P1} = L_{P2}$) and C_P] and a series resonator (L_S and C_S). The differential input currents (I_+ and I_-) are generated by the Gilbert mixer. By definition, the element D of the ABCD matrix (1) represents the current gain from port-1 to port-2 when port-1 is short-circuited.

$$D \equiv \frac{I_2}{I_1}\Big|_{V_1=0} = 1 + \frac{L_S}{L_P} + \frac{C_P}{C_S} - \omega^2(C_P L_S) - \frac{1}{\omega^2 C_S L_P} \qquad (1)$$

The current reversal occurs when $D = -1$ and $I_2 = -I_+ = -I_1$. Thus, the total combined current (I_{tot}) is doubled, that is, ideally 6 dB gain improvement, when compared with each output node of the Gilbert mixer. This mechanism is achieved at two frequencies by solving $D = -1$.

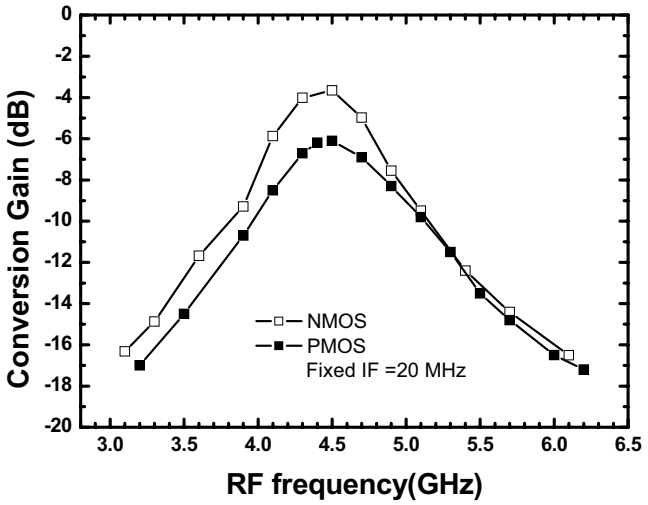

(a)

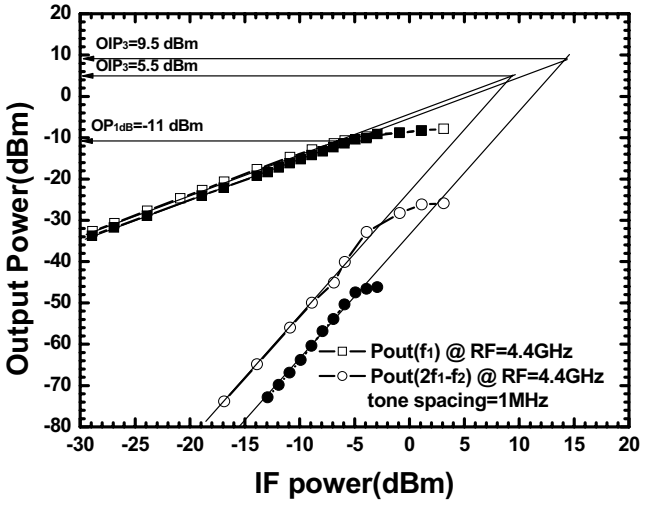

(b)

Figure 6 (a) Conversion gain with respect to RF frequency and (b) power performance of the high linearity Gilbert upconverters using NMOS/PMOS bias-offset TCAs and the LC current combiner

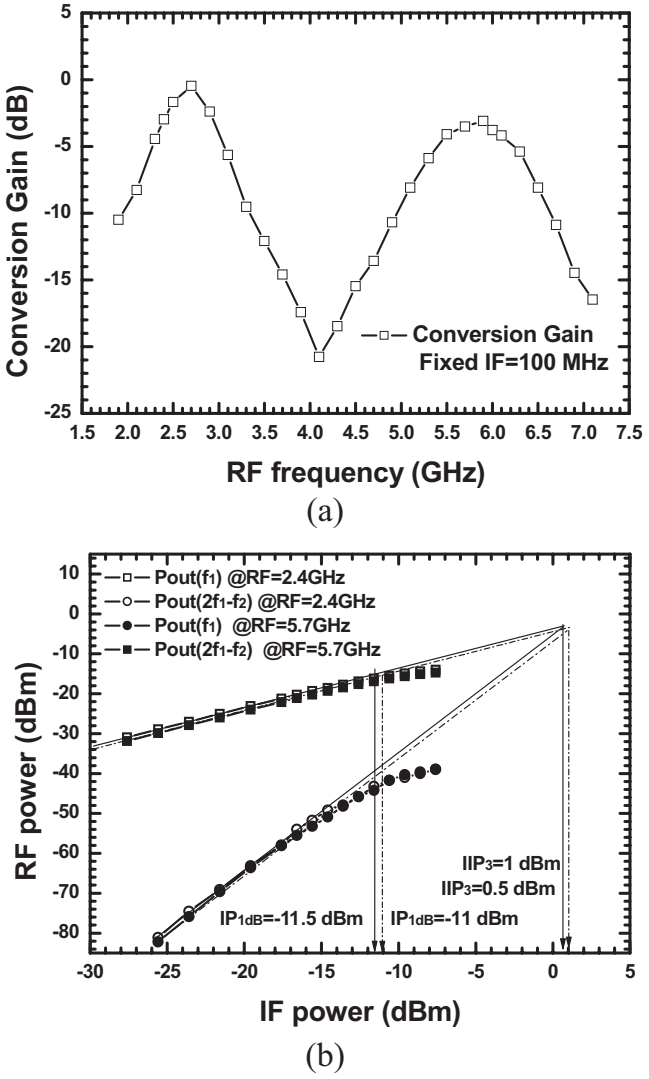

Figure 7 (a) Conversion gain with respect to RF frequency and (b) power performance of the dual-band Gilbert upconverter at RF = 2.4 and 5.7 GHz

For the application on WLAN 802.11a/g, the two frequencies are specified as $f_1 = 2.4$ GHz and $f_2 = 5.7$ GHz, respectively. The series capacitor C_S is decomposed into two capacitors with capacitance of $2C_S$ and these two capacitors are connected to each end of the floating inductor L_S for fully symmetric layout design. The lower limitation of inductances L_S and L_P are constraint by the achievable f_{Qmax} in practice while the capacitances of C_S and C_P are restricted by the severe parasitic effects. Consequently, in this work, $2C_S = 0.8$ pF and $C_P = 1$ pF and the inductances of L_P and L_S are 1.85 nH and 4.6 nH, respectively. In the dual-band LC current mirror, a center-tapped symmetric differential inductor (L_{P1}–L_{P2}) is composed of a five-square-turn inductor with the line width, spacing, and outer diameter of 4 μm, 2.5 μm, and 120 μm, respectively. The other symmetric inductor of L_S has the 3-μm line width, 3-μm line spacing, and 120-μm outer diameter. The die size is 1×1 mm^2. Moreover, the power improvement of the Gilbert upconverter is achieved by using the active matching network, the Darlington voltage buffer, in the output stage when compared with using a passive matching network.

The photograph of the high linearity Gilbert upconverters are demonstrated in this article by utilizing NMOS and PMOS TCAs are shown in Figures 5(a) and 5(b), whereas photograph of the dual-band upconverter is shown in Figure 5(c).

3. MEASUREMENT RESULTS AND CONCLUSION

The SiGe BiCMOS high linearity upconverters facilitate on-wafer RF measurements. The peak conversion gain of the upconverters with NMOS/PMOS input TCAs occurs at both RF = 4.4 GHz, IF = 20 MHz, and the LO power is −5 dBm as shown in Figure 6(a). The power performance of the upconverters with NMOS/PMOS TCAs is shown in Figure 6(b). The OP_{1dB} and OIP_3 are −11/−11 dBm and 5.5/9.5 dBm for the upconverters with NMOS and folded PMOS TCAs, respectively. Therefore, the difference between the OIP_3 and OP_{1dB} of the upconverters with NMOS/PMOS TCAs are 16.5 and 20.5 dB, whereas a conventional Gilbert upconverter has only 10-dB difference between the OIP_3 and OP_{1dB} [10, 11]. The IF bandwidth of the upconverters with NMOS and PMOS TCAs are 500 MHz and 100 MHz, respectively. The output RF return loss is better than 16 dB for both circuits over 20 GHz. The LO-to-RF isolation of each upconverter is better than 28/26 dB when LO frequency ranging from 4–5.2 GHz. The power consumption of each circuit is 40/46 mW, respectively.

Figure 7(a) shows the conversion gain with respect to RF output frequency when IF = 100 MHz. The measured conversion gain at desired frequencies of 2.4/5.7 GHz is −3/−3.5 dB with the *LO* input power of −4 dBm. However, the peak conversion gain is 0/−3 dB at 2.7/5.9 GHz due to the process variation. As shown in Figure 7(b), the dual-band upconverter has the IP_{1dB} of −11.5/−11 dBm, and the IIP_3 of 0.5/1 dBm when IF = 100 MHz, RF = 2.4 GHz, and 5.7 GHz, respectively. The power consumption is 49.5 mW at a 3.3-V supply.

ACKNOWLEDGMENTS

This work is supported by National Science Council of Taiwan, Republic of China under contract numbers NSC 95–2221-E-009–043-MY3, by the Ministry of Economic Affairs of Taiwan under contract number 96-EC-17-A-05-S1- 020, and by MoE ATU Program under contract number 95W803. The authors would like to thank National Chip Implementation Center (CIC) for the technical support.

REFERENCES

1. F. Ellinger, 26.5–30-GHz resistive mixer in 90-nm VLSI SOI CMOS technology with high linearity for WLAN, IEEE Trans Microwave Theory Tech 53 (2005), 2559–2565.
2. H.-K. Chiou, Y.-R. Juang, and H.-H. Lin, Miniature MMIC star double balanced mixer using lumped dual balun, Electron Lett 33 (1997).
3. A.S. Sedra and K.C. Smith, Microelecronic circuits, 4th ed., Oxford, New York, 2004, pp. 691–692.
4. B. Gilbert, The multi-tanh principle: A tutorial overview, IEEE J Solid State Circuits 33 (1998), 2–17.
5. Z. Wang and W. Guggenbuhl, A voltage-controllable linear MOS transconductor using bias offset technique, IEEE J Solid State Circuits 25 (1990), 315–317.
6. E. Seevinck and R.F. Wassenarr, A versatile CMOS linear transconductor/square-law function circuit, IEEE J Solid State Circuits SC-22 (1987), 366–377.
7. T.H. Wu, C. Meng, T.H. Wu, and G.W. Huang, A 5.7GHz Gilbert upconversion mixer with an LC current combiner output using 0.35 um SiGe HBT Technology, IEICE Trans Electron E88-C (2005), 1267–1270.
8. T.H. Wu, C.C. Meng, T.H. Wu, and G.W. Huang, A fully integrated 5.2 GHz SiGe HBT upconversion micromixer using lumped balun and LC current combiner, IEEE MTT-S Int Microwave Symp, Long Beach, CA (2005), 12–17.
9. K.L. Fong and R.G. Meyer, High frequency nonlinearity of common-

cmitter and differential-pair transconductance stages, IEEE J Solid State Circuits 33 (1998), 548–555.
10. G. Grau, U. Langmann, W. Winkler, D. Knoll, J. Osten, and K. Pressel, A current-folded up-conversion mixer and VCO with center-tapped inductor in a SiGe-HBT technology for 5-GHz wireless LAN applications, IEEE J Solid State Circuits 35 (2000), 1345–1352.
11. J.P. Comeau and J.D. Cressler, A 28-GHz SiGe up-conversion mixer using a series-connected triplet for higher dynamic range and improved IF port return loss, IEEE J Solid State Circuits 41 (2006), 560–565.

A MINIATURE X-BAND-EMBEDDED MULTILAYER BAND-PASS FILTER USING LTCC TECHNOLOGY

Zhigang Wang, Bo Yan, Ruimin Xu, and Weigan Lin
School of Electronic Engineering, University of Electronic Science and Technology of China, Chengdu 610054, People;s Republic of China; Corresponding author: zgwang@ee.uestc.edu.cn

Received 13 October 2008

ABSTRACT: *This article proposes a miniature embedded multilayer interdigital bandpass filter (BPF) based on low temperature co-fired ceramic (LTCC) technology, which is used to suppress fundamental and harmonic components of local-oscillator signal in a LTCC transceiver module. A practical design methodology corresponding to LTCC multilayer configuration is described. A five-order Chebyshev interdigital BPF is developed and verified by full-wave simulation. The proposed filter is fabricated using multilayer LTCC technology and measured using vector network analyzer. Good agreement between simulated and measured response is observed. Covering area of the fabricated BPF is only 8.1 × 7.4 mm² (including via fences).* © 2009 Wiley Periodicals, Inc. Microwave Opt Technol Lett 51: 1722–1725, 2009; Published online in Wiley InterScience (www.interscience.wiley.com). DOI 10.1002/mop.24432

Key words: *BPF; LTCC; LO; transceiver; multilayer configuration*

1. INTRODUCTION

Increasing demands of making communication systems lighter, more compact, and with better functionality, set many challenges for packaging and structure configuration. LTCC technology gives a new design conception and method to solve these problems [1, 2]. By embedding passive components into multiplayer substrate and mounting active elements on the surface layer, LTCC technology offers opportunity to realize very compact systems, such as LTCC transmitters, receivers, or complicated transceiver modules [3, 4].

LTCC bandpass filter (BPF) is a key component in these modules [5]. When the frequency is not high, LTCC filters are usually implemented by LC-element type. With increasing of frequency, the effects of parasitics deteriorate performance of such filters. So, coupling resonator or cavity bandpass filter realized in LTCC multilayer substrate was widely used in the LTCC microwave and millimeter-wave modules [6].

In this article, a feed-in RF signal (4.75 GHz) was octupled up to millimeter-wave frequency (38 GHz), as local-oscillator (LO) signal in the LTCC transceiver module, as shown in Figure 1. After first doubling, second-order harmonic is needed, but the leaking fundamental (4.75 GHz) and 3rd order harmonic (14.25 GHz) components should be suppressed at least 40 dB by BPF. At the same time, BPF must be incorporated with the whole LTCC module. Therefore, an embedded LTCC BPF was designed for this application.

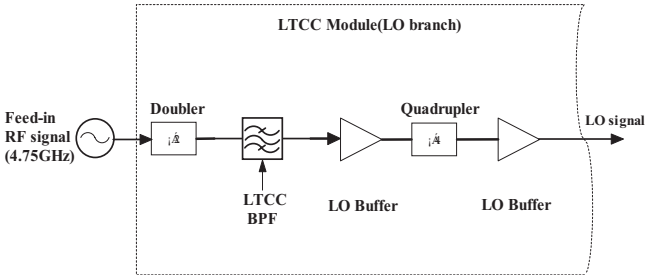

Figure 1 The block diagram of LO branch in LTCC transceiver module

2. ANALYSIS

The classical design theories of filter have been consummated since long time ago [7–9]. For symmetric coupling structure, even- and odd-mode analyze is widely used. However, this method is not applicable for asymmetric coupled line buried in different layers. In this section, a practical design method is presented, which is based on EM simulation extraction of external quality factor Q_e and coupling coefficient K_{ij}. First of all, the element values for Chebyshev lowpass prototype can be calculated as follows [10]:

$$\begin{cases} g_0 = 1.0, g_1 = \dfrac{2\sin\dfrac{\pi}{2n}}{r} \\ g_i g_{i-1} = \dfrac{4\sin\dfrac{(2i-1)\pi}{2n}\sin\dfrac{(2i-3)\pi}{2n}}{\gamma^2 + \sin^2\dfrac{(i-1)\pi}{n}}, \text{for } i = 2,3,\ldots n \\ g_{n+1} = 1(n\_\text{odd}) \text{ or } \coth\left(\dfrac{\beta}{4}\right)(n\_\text{even}) \end{cases} \quad (1)$$

Where $\beta = \ln\left[\coth\left(\dfrac{L_{Ar}}{17.37}\right)\right]$, $\gamma = \sinh\left(\dfrac{\beta}{2n}\right)$
then, the design parameters of BPF, that is, the coupling coefficient (K_{ij}) and external quality factor (Q_e), can be determined by the formulas:

$$Q_{ei} = Q_{eo} = \frac{g_0 g_1}{\text{FBW}} \quad (2)$$

$$K_{i,i+1} = \frac{\text{FBW}}{\sqrt{g_i g_{i+1}}} \text{ for } i = 1 \text{ to } (n-1)$$

Where g_i 's are the element values of Chebyshev lowpass prototype filter, FBW is the fractional bandwidth, and n is the order of the filter.

Relationship between these parameters and filter's physical dimensions can be made by

$$\begin{cases} Q_e = \dfrac{\omega_0}{\Delta\omega_{\pm 90^\circ}} \\ K = \dfrac{f_{p2}^2 - f_{p1}^2}{f_{p2}^2 + f_{p1}^2} \end{cases} \quad (3)$$

ω_0 is center frequency of BPF, $\Delta\omega_{\pm 90^\circ}$ can be determined from the frequency at which the phase of S_{11} shifts $\pm$ 90° with respect to